J Electroceram (2006) 16:575–579
DOI 10.1007/s10832-006-9922-0

Cracking of low temperature solution deposited CeO_2 thin films

Gregory K. L. Goh · Christine S. S. Tay · Kelvin Y. S. Chan · N. Gosvami

Abstract Crystalline CeO_2 films grown in aqueous solutions at 45°C on glass slides formed by the island growth mode. The film had a refractive index of 1.83 and indicated that the film had a porosity of 41.3%, which significantly lowered the elastic stiffness of the film. The film cracked only after drying in a mud crack pattern when it reached a critical thickness. This indicated that the film cracked under tensile stress due to the accumulation of tensile strains generated from grain coalescence during growth, thermal expansion mismatch during cooling and capillary stress during drying.

Keywords CeO_2 · Porosity · Film cracking

1 Introduction

Ceria (CeO_2) films have important applications as a gate oxide in MOS devices [1], corrosion resistant coatings in aqueous environments and high temperatures [2, 3], UV absorbing coatings and as an electrolyte in solid oxide fuel cells (SOFC) [4]. Ceria films are important as an alternative to chromate films for corrosion protection because CeO_2 has very low toxicity [5] while the chromates can be carcinogenic [6]. In addition, the use of ceria-based anodes promotes hydrocarbon oxidation and has aided in the development of direct methane SOFC [7]. Therefore, it is clear that low cost methods for depositing CeO_2 films will be beneficial to industry.

Presently, CeO_2 films can be grown by vapor deposition methods like pulsed laser deposition [1], magnetron sputtering [8] and evaporation [9] and also solution methods like sol-gel spin coating [10], electrodeposition [11], oxidative-soak-coating [12] and successive-ionic-layer-adsorption-and-reaction (SILAR) [13]. Besides being capital intensive, the vapor deposition methods normally require substrate temperatures of 600°C and above. For the solution methods, sol-gel requires elevated temperatures (>450°C) for post deposition crystallization while electrodeposition is limited to conducting substrates.

To date, the remaining low cost and low temperature methods of oxidative-soak-coating and SILAR both have a film thickness limitation of about 60 nm. For SILAR, it is believed that dissolution of the film in the growth solution is the limiting factor [13] while poor adhesion appeared to be the reason why thicker films could not be grown by the oxidative-soak-coating method [12]. These low temperature film growth methods offer unique material combinations not attainable with high temperature methods (e.g. polymeric substrates with refractory ceramic coatings) and the use of solutions enable uniform deposition on irregular or even porous bodies not possible with the line-of-sight vapor deposition methods mentioned earlier. Therefore, it is important to understand the cause of the film thickness limitation that is preventing greater use of these methods in the case of ceria. This study will focus on the oxidative-soak-coating method, for which it was observed that the ceria film actually cracks first before spalling off. The various sources of strain during film growth, cooling and drying will be examined to determine if the critical thickness above which film cracking occurs coincides with the experimentally observed value.

2 Experimental details

Crystalline CeO_2 films were deposited on borosilicate glass slides by the oxidative soak coating method [12]. Briefly,

G. K. L. Goh (✉) · C. S. S. Tay · K. Y. S. Chan · N. Gosvami
Institute of Materials Research and Engineering, 3 Research Link, Singapore 117602, Singapore
e-mail: g-goh@imre.a-star.edu.sg

$Ce(CH_3COO)_3$ and $KClO_3$ were dissolved in deionized water giving 0.01 M of $Ce(CH_3COO)_3$ and 0.02 M of $KClO_3$. The glass slide was placed at the bottom of a 45 ml Teflon-lined, stainless steel hydrothermalreactor (Parr) containing the precursor solution. The reactor was then capped tightly and placed into a drying oven at 45°C for the required heating period. After the reaction, the films were rinsed repeatedly with deionised water and dried at room temperature.

The morphology of the films was examined by scanning electron microscopy (JEOL 6300F), optical microscopy and also by atomic force microscopy (Molecular Imaging). Images were acquired in contact mode using a commercial silicon nitride probe (Olympus) with a spring constant of 0.36 Nm^{-1}. The sample and cantilever were completely immersed in an inert liquid (phenyloctane) during imaging to minimize capillary forces and contamination in order to achieve better image resolution. The deflection signal of the cantilever acquired was representative of the topography of the sample. The refractive index and thickness of the film were determined by variable angle spectroscopic ellipsometry (VASE) while surface profilometry (Tencor P-10) was used to determine film thicknesses above 100 nm.

3 Results and discussion

3.1 Film growth and cracking

As is commonly observed for films grown by low temperature solution methods [14, 15], the CeO_2 film in this study formed by an island growth mode (Volmer-Weber). After coalescence, the film started showing signs of cracking around 24 h of growth (Fig. 1). At this stage, the film was 80 nm thick (as determined by ellipsometry) and the average diameter of the islands was approximately 20 nm, as shown in Fig. 2. When a film previously grown for 24 h was reintroduced into a fresh precursor solution for another 24 h to grow a much thicker film (200 nm as determined by surface profilometry), film cracking was even more pronounced, and pieces of the film began spalling off (not shown). These observations indicated that the film thickness limitation associated with the oxidative soak coating method was due to the accumulation of strain energy that eventually led to film cracking. Cracking began at the film surface, propagated through the film to the substrate and then along the interface, causing film spallation.

The 'mud crack' type pattern observed indicates that the film cracked as a result of a biaxial tensile stress [16]. Since biaxial tensile stresses can be generated during film growth, when the film is cooling to room temperature after growth and when the film is drying, determining the point at which the film cracked gives an idea of the strain mechanisms involved in film cracking. Observations with an optical microscope indicated that the crack openings for the 24 h film (see Fig. 1(a)) were not large enough for observation under optical wavelengths. Fortunately the cracks in the film grown for two 24 h cycles were observable under the optical microscope.

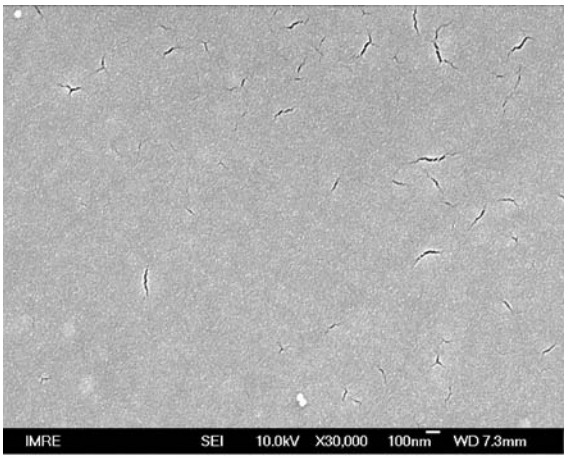

(a)

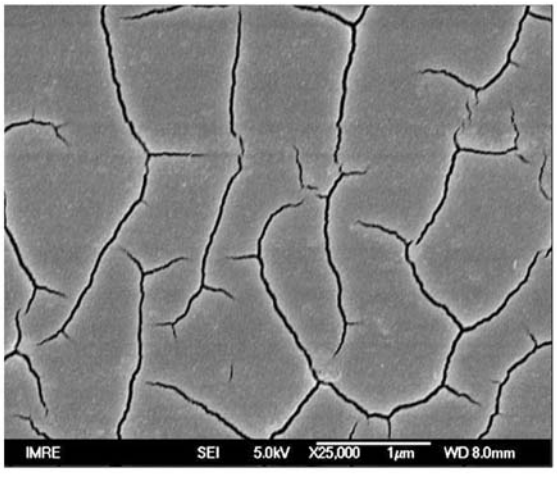

(b)

Fig. 1 SEM of CeO_2 films deposited at 45°C after (a) one 24 h cycle, and (b) two 24 h cycles

Therefore, it was carefully ensured that a film grown for two 24 h cycles was kept immersed in solution in between cycles and then observed by optical microscopy at room temperature after the second cycle, while still immersed in the growth solution. This observation is shown in Fig. 3(a). Figure 3(b) shows the same film after it was dried, displaying the familiar mud crack pattern previously observed in Fig. 1(b) and indicates that the film did not crack after the growth or cooling stages, but only after the drying stage. This in turn suggests that the cumulative tensile strain developed during the growth, cooling and drying stages contributed to film cracking.

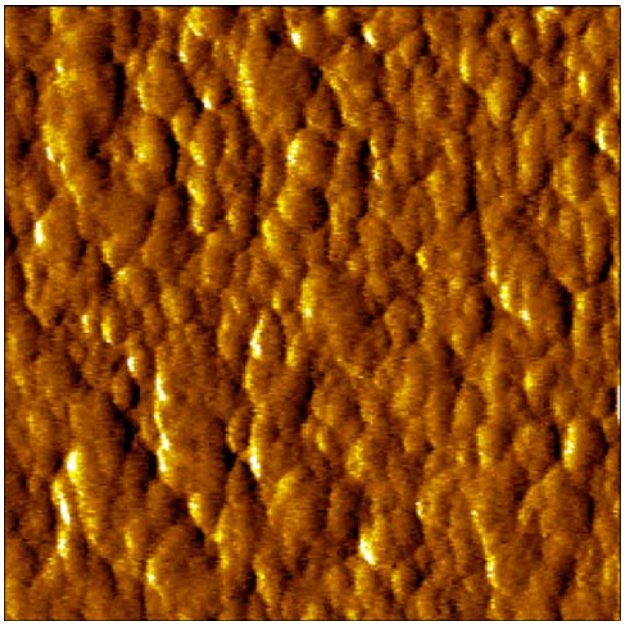

Fig. 2 Deflection mode AFM of the single cycle 24 h film (400 × 400 nm scan size)

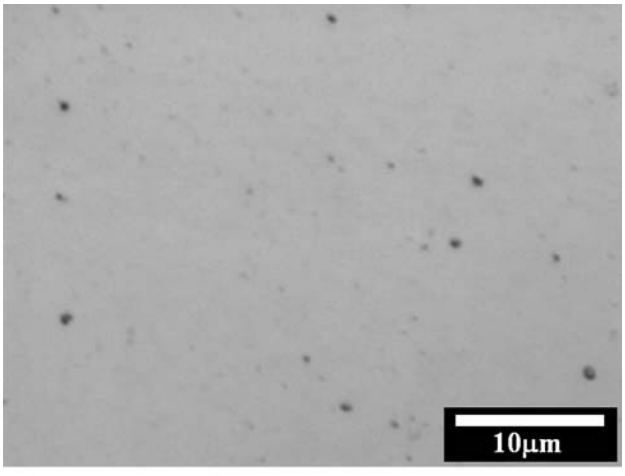

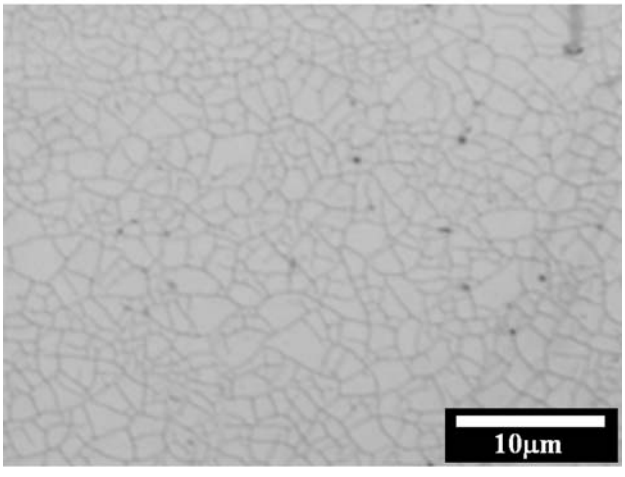

Fig. 3 Optical micrographs of the CeO_2 film grown after two 24 h cycles (a) while still submerged in solution, and (b) after drying

3.2 Porosity

In the next section, the strains developed during the various stages (growth, cooling and drying) are calculated in order to determine the critical thickness above which film cracking should occur as compared to the experimentally observed critical thickness. Before this is done, the amount of porosity in the film will be determined by comparing the experimentally observed refractive index with values reported in the literature for dense CeO_2 films. This is important as the film's Young's modulus is significantly affected by porosity, p, according to Eq. (1) [17],

$$E_p = E(1-p)^2 \tag{1}$$

where E_p is the Young's modulus of the porous film and E is the Young's modulus for the bulk material (172 GPa) [18].

Figure 4 shows the variation of the refractive index of the 24 h film with wavelength. At a wavelength of 632.8 nm, the film had a refractive index, n, of 1.83 which is significantly lower than that observed for a dense CeO_2 film ($n_f = 2.47$) [8]. This reduction in refractive index was due to the presence of pores in the film. The porosity, p, in the film was determined using the Bruggeman effective medium approximation (EMA) [19],

$$(1-p)\frac{n_f^2 - n^2}{n_f^2 + 2n^2} + (p)\frac{n_v^2 - n^2}{n_v^2 + 2n^2} = 0 \tag{2}$$

where the refractive index for voids filled with air, n_v, was taken as 1. This resulted in a porosity, p, of 0.413 that lowered the Young's modulus from 172 GPa to 59.3 GPa according to Eq. (1).

Likely locations for the pores are at the junctions of the coalesced islands. As proposed by Goh and co-workers [16],

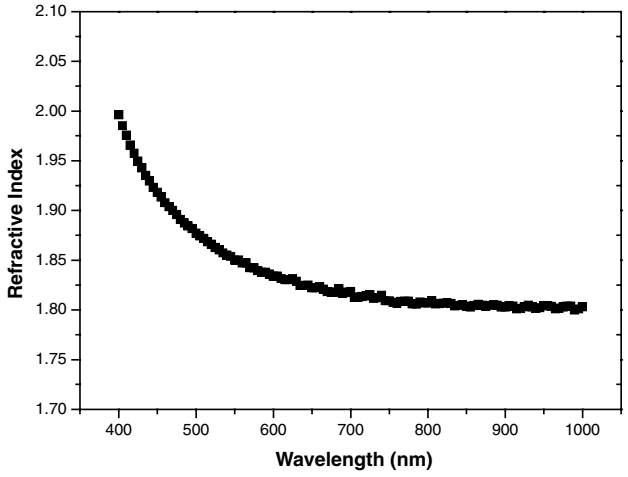

Fig. 4 Refractive index of the CeO_2 film grown at 45°C after 24 h

the radius of such a pore, r, can be estimated from a simple geometrical relationship between circular islands of radius R surrounding the pore from,

$$(R + r)\cos 30^\circ = R \tag{3}$$

A reasonable estimate from Fig. 2 is an average island radius, R, of 10 nm and this results in a pore radius, r, of 1.55 nm.

3.3 Sources of strain

In the Volmer-Weber mode of growth, individual islands nucleate on the substrate, grow, approach and impinge on adjacent islands, eventually coalescing to form a continuous film. As first proposed by Hoffman [20], approaching islands with a small gap between them deform slightly and spontaneously snap together, forming a relatively lower energy grain boundary in place of the two adjacent island free surfaces prior to coalescence. As such, this coalescence results in an average tensile stress, which for a film with approximately hemispherical grains at the point of coalescence, can be expressed using the following equation [21],

$$\sigma_{\text{ave}} = \frac{4}{R}\left(\gamma_s - \frac{1}{2}\gamma_{gb}\right) \tag{4}$$

where R is the average radius of the islands and γ_s and γ_{gb} are the free energies of the island surface and grain boundaries respectively. For a film under plane stress, the corresponding strain is given by,

$$\varepsilon_1 = \frac{4}{R}\frac{(1-\nu)}{E_p}\left(\gamma_s - \frac{1}{2}\gamma_{gb}\right) \tag{5}$$

where ν is the poisson's ratio. Using an order of magnitude estimation of 1 J/m^2 for $(\gamma_s - \frac{1}{2}\gamma_{gb})$, $R = 10$ nm and $\nu = 0.3$ [18], the tensile strain due to grain coalescence, ε_1, is estimated to be about 4.72×10^{-3}.

During the cooling phase from 45°C to room temperature (25°C), any mismatch in the thermal expansion coefficients (CTE) of the film and substrate can generate a residual strain according to,

$$\varepsilon_2 = \int_{T_i}^{T_f} (\alpha_{\text{film}} - \alpha_{\text{substrate}})dT \tag{6}$$

where $T_f = 25^\circ$C, $T_i = 45^\circ$C, $\alpha_{\text{film}} = 11.6 \times 10^{-6}$ K^{-1} [22] and $\alpha_{\text{substrate}} = 3.3 \times 10^{-6}$ K^{-1} [23] are the thermal expansion coefficients of the film and substrate respectively. Since the CTE of the film is larger than that for the substrate and the substrate is much thicker than the film, the resultant tensile strain, $\varepsilon_2 = 1.66 \times 10^{-4}$, will reside completely in the film.

As mentioned earlier in Section 3.2, the coalescence of islands can lead to the presence of porosity at the junction between islands. In the solution growth of highly oriented TiO_2 films at 60°C [8], such pores were responsible for the generation of tensile stresses during film drying. This is because the pressure difference across the liquid-vapour interface (meniscus) of the solvent in the pore during drying generates a capillary stress that tends to contract the film. As the substrate prevents the film from contracting, a tensile stress is set up. The magnitude of this tensile strain can be determined from the Laplace equation ($\sigma = 2\gamma/r$) according to,

$$\varepsilon_3 = \frac{(1-\nu)}{E_p}\frac{2\gamma_w}{r} \tag{7}$$

where the surface tension of water, $\gamma_w = 72 \times 10^{-3}$ J/m^2 and the pore radius, $r = 1.55$ nm (see Section 3.2). This gives a tensile strain due to capillary forces, ε_3, of 1.10×10^{-3}.

Therefore the residual tensile strain accumulated up to this point is given by, $\varepsilon_r = \varepsilon_1 + \varepsilon_2 + \varepsilon_3 = 5.986 \times 10^{-3}$. The resultant tensile stress due to this accumulated strain can be relieved by the propagation of cracks that form a mud crack pattern. As the strain energy stored in the film increases with film thickness, there is a critical thickness, h_c, above which cracking will occur to relieve the film stress. This critical value is given by [24],

$$h_c = \frac{\Gamma E_p}{Z\sigma^2(1-\nu^2)} \tag{8}$$

where the fracture resistance, $\Gamma = K_{Ic}^2(1-\nu^2)/E_p$ and $\sigma = E_p\varepsilon_r/(1-\nu^2)$. Z is a dimensionless parameter that depends on the cracking geometry and has a value of 3.951 when cracks first form. Using a value of 1.4 MPa$m^{\frac{1}{2}}$ for K_{Ic} [25], Eq. (8) reveals that the film should only crack for film thicknesses above 3.26 μm. This is about 40 times larger than the experimentally observed value of 80 nm (i.e. for 24 h of growth).

There are several factors that could have contributed to this discrepancy. Firstly, it has been observed in nano-sized ceria that there is significant lattice expansion. This expansion is due to the lowering of valence of the cerium ion from 4+ to 3+ which leads to a reduction in the Coulombic attractive forces in the lattice, that is, a weakening of the elastic stiffness [26]. Reduction in the attractive forces leading to lattice expansion has also been observed for solution synthesized material, but due to proton incorporation instead [27, 28]. Secondly, lowering of the cerium valence requires the presence of oxygen vacancies to maintain charge neutrality. The presence of oxygen vacancies in the film would be another source of tensile strain. Finally, the effect of porosity on the fracture toughness, K_{Ic}, of the film has not been taken into account. It would be reasonable to assume that a more

porous material would have lower fracture toughness than its denser counterpart. All these factors, if taken into account, would lead to a lower calculated critical thickness that may be more agreeable with the experimentally observed value.

4 Conclusions

It was observed that CeO_2 films grown by the oxidative-soak-coating method at 45°C on borosilicate glass slides formed by the island growth mode, with an average island size of 20 nm. Comparison of the film refractive index of 1.83 with that for dense CeO_2 films indicated that the film had a high degree of porosity of 41.3%. This significantly lowered the elastic stiffness of the film and magnified strains developed at various stages of the entire film growth process. The film cracked in a mud crack pattern when it reached a critical thickness, but only after drying. Mud cracking indicated that the film cracked under tensile stress while the latter observation indicated that the tensile stress that caused cracking was a result of the accumulation of tensile strains generated from grain coalescence during growth, thermal expansion mismatch during cooling and capillary stress from the removal of the wash solvent during drying.

References

1. J. Lappalainen, D. Kek, and H.L. Tuller, *J. Eur. Ceram. Soc.*, **24**, 1459 (2004).
2. A.E. Hughes, R.J. Taylor, B.R.W. Hinton, and L. Wilson, *Surf. Interf. Anal.*, **23**(7/8), 540 (1995).
3. S. Roure, F. Czerwinski, and A. Petric, *Oxid. Metals*, **42**(1/2), 75 (1994).
4. T. Mori, J. Drennan, J.-H. Lee, J.-G. Li, and T. Ikegami, *Solid State Ionics*, 154–155, 461 (2002).
5. N. Irving Sax and R.J. Lewis Sr., *Dangerous Properties of Industrial Materials*, 7th edition, vol. 2 (Van Nostrand Reinhold, New York, 1989), p. 743.
6. *Toxicology Profile for Chromium*, ATDSR/TP-88/10, Agency for Toxic Substances, US. Public Health Service (1989).
7. E.P. Murray, T. Tsai, and S.A. Barnett, *Nature*, **400**, 649 (1999).
8. S. Guo, H. Arwin, S.N. Jacobsen, K. Jarrendahl, and U. Helmersson, *J. Appl. Phys.*, **77**(10), 5369 (1995).
9. S. Logothetidis, P. Patsalas, E.K. Evangelou, N. Konofaos, I. Tsiaoussis, and N. Frangis, *Mater. Sci. Eng. B*, **109**, 69 (2004).
10. N. Ozer, *Solar Energy Mater. Solar Cells*, **68**, 391 (2001).
11. I. Zhitomirsky and A. Petric, *Ceram. Int.*, **27**, 149 (2001).
12. H. Unuma, T. Kanehama, K. Yamamoto, K. Watanabe, T. Ogata, and M. Sugawara, *J. Mater. Sci.*, **38**, 255 (2003).
13. V.P. Tolstoy and A.G. Erlich, *Thin Solid Films*, **307**, 60 (1997).
14. G.K.L. Goh, C.G. Levi, and F.F. Lange, *J. Mater. Res.*, **17**(11), 2852 (2002).
15. G.K.L. Goh and S.K. Donthu, in: *Perovskite Materials*, edited by K. Poeppelmeier, A. Navrotsky, and R. Wentzcovitch (Materials Research Society, San Francisco, 2002), D10.13.
16. G.K.L. Goh, S.K. Donthu, and P.K. Pallathadka, *Chem. Mater.*, **16**, 2857 (2004).
17. O. Belmont, D. Bellet, and Y. Brechet, *J. Appl. Phys.*, **79**(10), 7586 (1996).
18. J.F. Shackelford, *CRC Materials Science, and Engineering Handbook*, 3rd edition (CRC Press, Boca Raton, 2001).
19. C.H. Peng and S.B. Desu, *J. Am. Ceram. Soc.*, **77**(4), 929 (1994).
20. R.W. Hoffman, *Thin Solid Films*, **34**, 185 (1976).
21. L.B. Freund and E. Chason, *J. Appl. Phys.*, **89**(9), 4866 (2001).
22. A.K. Tyagi, B.R. Ambekar, and M.D. Mathews, *J. Alloys Compd.*, **337**, 277 (2002).
23. W.D. Callister Jr., *Materials Science, and Engineering: An Introduction*, 4th edition (Wiley, New York, 2003), p. 646.
24. E.V. Etzkorn and D.R. Clarke, *J. Appl. Phys.*, **89**(2), 1025 (2001).
25. S. Maschio, O. Sbaizero, and S. Meriani, *J. Eur. Ceram. Soc.*, **9**, 127 (1992).
26. S. Tsunekawa, K. Ishikawa, Z.-Q. Li, Y. Kawazoe, and A. Kasuya, *Phys. Rev. Lett.*, **85**(16), 3440 (2000).
27. G.K.L. Goh, S.M. Haile, C.G. Levi, and F.F. Lange, *J. Mater. Res.*, **17**(12), 3168 (2002).
28. G.K.L. Goh, F.F. Lange, S.M. Haile, and C.G. Levi, *J. Mater. Res.*, **18**(2), 338 (2003).